OAK RIDGE
NATIONAL LABORATORY

MANAGED BY UT-BATTELLE
FOR THE DEPARTMENT OF ENERGY

ORNL/TM-2004/53

Quantitative Determination of Gamma-Emitting Nuclide Contents Using Energy-Dependent Photon Attenuation

June 2006

A. M. Krichinsky
A. J. Lucero
P. J. Bereolos
J. S. Bogard
C. S. Scheffing

UT-BATTELLE
ORNL-27 (2-03)

DOCUMENT AVAILABILITY

Reports produced after January 1, 1996, are generally available free via the U.S. Department of Energy (DOE) Information Bridge:

Web site: http://www.osti.gov/bridge

Reports produced before January 1, 1996, may be purchased by members of the public from the following source:

National Technical Information Service
5285 Port Royal Road
Springfield, VA 22161
Telephone: 703-605-6000 (1-800-553-6847)
TDD: 703-487-4639
Fax: 703-605-6900
E-mail: info@ntis.fedworld.gov
Web site: http://www.ntis.gov/support/ordernowabout.htm

Reports are available to DOE employees, DOE contractors, Energy Technology Data Exchange (ETDE) representatives, and International Nuclear Information System (INIS) representatives from the following source:

Office of Scientific and Technical Information
P.O. Box 62
Oak Ridge, TN 37831
Telephone: 865-576-8401
Fax: 865-576-5728
E-mail: reports@adonis.osti.gov
Web site: http://www.osti.gov/contact.html

This report was prepared as an account of work sponsored by an agency of the United States Government. Neither the United States government nor any agency thereof, nor any of their employees, makes any warranty, express or implied, or assumes any legal liability or responsibility for the accuracy, completeness, or usefulness of any information, apparatus, product, or process disclosed, or represents that its use would not infringe privately owned rights. Reference herein to any specific commercial product, process, or service by trade name, trademark, manufacturer, or otherwise, does not necessarily constitute or imply its endorsement, recommendation, or favoring by the United States Government or any agency thereof. The views and opinions of authors expressed herein do not necessarily state or reflect those of the United States Government or any agency thereof.

ORNL/TM-2004/53

Nuclear Science and Technology Division

Quantitative Determination of Gamma-Emitting Nuclide Contents Using Energy-Dependent Photon Attenuation

A. M. Krichinsky
A. J. Lucero*
P. J. Bereolos†
J. S. Bogard‡
C. S. Scheffing**

Date Published: June 2006

Prepared by the
OAK RIDGE NATIONAL LABORATORY
Oak Ridge, Tennessee 37831-6283
managed by
UT-BATTELLE, LLC
for the
U.S. DEPARTMENT OF ENERGY
under contract DE-AC05-00OR22725

*Western Research Institute, Laramie, Wyo.
†Select Engineering and Contracting, Inc., Knoxville, Tenn.
‡Life Sciences Division, ORNL.
**Former DOE Student Undergraduate Laboratory Internships participant at ORNL.

CONTENTS

LIST OF FIGURES v

LIST OF TABLES v

ACKNOWLEDGMENTS vii

ABSTRACT ix

1. INTRODUCTION 1

2. METHODOLOGY 2
   - 2.1 Methodology Overview 2
   - 2.2 Measured Activity and Data Normalization 2
   - 2.3 Attenuation-Corrected Measurement Equation 4
   - 2.4 Photon Peak Selections 8
   - 2.5 Estimating Activity 10

3. EQUIPMENT 12

4. DATA ANALYSIS 13
   - 4.1 Results 13
   - 4.2 Uncertainty 16
   - 4.3 Discussion of Results 20

5. CONCLUSIONS 23

6. REFERENCES 25

LIST OF FIGURES

Figure		Page
1	Radioactive decay series for ^{232}U	3
2	Plot of the mass attenuation coefficient with $1/E$ for common packaging materials (glass, aluminum, iron), detector material (germanium), and uranium itself (U, U_3O_8). The regression line is for iron	6
3	Attenuation curves for high-purity ^{233}U	8

LIST OF TABLES

Table		Page
1	Values of the mass attenuation coefficient for some common shielding materials	5
2	Gamma peaks from ^{232}U decay progeny	9
3	NDA results for ^{232}U	14
4	NDA results for ^{233}U	17
5	Reported gamma-ray intensities	18
6	Some uncertainties related to estimated ^{233}U quantities	22

ACKNOWLEDGMENTS

The authors would like to acknowledge the following individuals for their assistance in preparing this report:

Charles W. Alexander and Robert L. Coleman, who provided valuable technical input used herein (including Fig. 1), and technically reviewed this report;

E. Steven Meyers and Michael W. Burgess, who performed measurements and collected much of the data that are summarized in the experimental portion of the report;

Bryce A. Powers, who was instrumental in early conceptual work that led to formulation of the attenuation model; and

Deborah S. Brown, Deborah K. Milsap, Marsha K. Savage, Deborah P. Stevens for administrative and editorial assistance in finalizing the report.

ABSTRACT

A promising technique allows gamma emissions to be used directly to measure quantities of fissile material — without prior knowledge or estimation of shielding provided by packaging, the contained material's characteristics, or the distribution of material within the containers. This measurement is the result of a simple, straightforward method that uses energy-dependent photon attenuation to model empirically the package attenuation from typical gamma spectra. The correction for attenuation is made possible by analyzing multiple emissions from the nuclide itself, its progeny, or from one or more commingled nuclides. An example is provided using a nuclide system involving ^{233}U and ^{232}U, which always accompany each other (in varying concentrations) and are commingled consistently with the material of interest (which is typical of isotopes in most process campaigns). As is typical of this nuclide system, the accompanying ^{232}U and its progeny reliably provide a broad spectrum of prominent gamma photopeaks — even in the presence of a prominent Compton Continuum. For progeny in secular equilibrium with a long-lived nuclide in the decay chain, a predictable relationship emerges between the measured activity from a particular emission and the energy of that emission. This relationship then may be used directly to estimate the quantity of material contained therein.

This method may be applied to quantifying any radioactive material having an associated broad spectrum of gamma photons (with energies from 0.1 to 3 MeV) — as long as the relative intensities of these emissions are known (for instance, where members of a decay chain are in secular equilibrium with a long-lived progeny).

Although the goal of this work is to provide a technique for *verifying* inventory values, its development thus far has provided estimations of contents that can be used only for *confirming* inventory values (a less precise measure than verification) or that can be used in estimating waste contents (rather than inventoried material).

1. INTRODUCTION

Nuclear material control and accountability (MC&A) requires direct measurements of accountable nuclides to quantitatively verify the contents of special nuclear materials (SNM). Nondestructive assay (NDA), as the name implies, allows such measurements without altering or damaging the package or the contained material. Passive NDA relies on the material's inherent emissions to provide a characteristic signal for quantifying contents. (This compares to active NDA, which probes the sample with a neutron field in order to induce gamma or neutron emissions that subsequently are measured) However, challenges in the use of passive NDA are presented by substantial self-attenuation of typically low-energy gamma photons emanating from ill-defined, high-density material matrices or, worse, essentially undefinable heterogeneous matrices. In some cases, this challenge is exacerbated by the presence of a strong Compton Continuum resulting from high-energy gamma emissions. This is the case for the $^{233}U/^{232}U$ system which is used as an example throughout this paper to demonstrate flexibility in applying the energy-dependent photon-attenuation methodology.

In the $^{233}U/^{232}U$ system, a strong Compton Continuum results from high-energy gamma photons emitted by ^{232}U progeny which is associated with the vast majority of ^{233}U. For materials with large relative amounts of ^{232}U, the Compton Continuum can totally swamp the prominent, low-energy gamma photopeaks (e.g., at 291.3, 317.16, and 320.54 keV) emanating directly from ^{233}U. However, for lower relative concentrations of ^{232}U [i.e., below ~20 parts per million (ppm) on a ^{233}U basis which encompasses the vast majority of ^{233}U in the nation's inventory], the strongest ^{233}U photopeak (at 317 keV), and sometimes the other two prominent peaks, can be detected reliably. (Two additional photopeaks have higher intensities than the one at 317 keV but are of much lower energies such that one is below the lower discrimination point and the other typically is obscured by the Continuum.) It is recognized that the 317-keV peak can be detected at higher relative concentrations of ^{232}U (i.e., above ~20 ppm) with substantially longer counting times that were not afforded this effort.

Current practices in compensating for self-attenuation typically involve an initial guess at the attenuation starting with selecting a candidate, pre-defined material to describe this attribute. Then an initial guess of the attenuation is selected (or interpolated from a series of pre-defined curves) as a candidate model to approximate this characteristic. (refs. 1, 2) Activities indicated from several photopeaks at selected energies for a specific nuclide are adjusted for the initial guess using attenuation's inverse relationship with energy. If the adjusted activities are approximately equal (or not monotonically different with respect to energy), then the average of these activities is used as the estimated activity for the nuclide. If the adjusted activities are not approximately equal (or if they demonstrate a monotonic relationship with energy), then another pre-defined material (or another interpolation) is selected to approximate attenuation. This process is repeated until the adjusted activities yield acceptable results (as indicated above). It also is significant that the quantities determined by these current practices consistently overestimate the contents being determined. This may be acceptable if the intent is to establish an upper bound for the content. *The methodology presented herein avoids the initial guessing or preselection of a presumed attenuating medium, and avoids overestimation of contents.*

2. METHODOLOGY

2.1 Methodology Overview

The technique described in this report addresses attenuation by modeling the matrix directly, using the broad energy range of selected gamma emissions representing identical activities. For ^{233}U, this involves decay products of ^{232}U, which are assumed to be in secular equilibrium with a long-lived progeny. The radioactive decay series of ^{232}U is shown in Fig. 1.

A first-order equation results from a regression of reported activities of ^{232}U radioactive progeny, based on the number of photon emissions (proportional to peak areas that are uncorrected for attenuation) at selected energies, against a function of the photon energy. In this equation, the y-intercept is equivalent to the logarithm of the true ^{232}U activity.

The slope of the equation developed for ^{232}U and the energy function in which this regression is linear are related directly to the inherent attenuating characteristics of the matrix and packaging from which the photons were emitted. The slope and energy function then may be used to generate a comparable regression equation for ^{233}U activity in the same matrix by using a prevalent ^{233}U photopeak (i.e., at 317 keV), thereby permitting direct estimation of the SNM quantity.

2.2 Measured Activity and Data Normalization

Gamma-ray photon spectra were collected and analyzed using GammaVision® software (from AMETEK® ORTEC.® (A minor objective was to use readily available output of existing spectral analysis software as direct input to this methodology). Activity estimates accounting for scattered background, source-to-detector distance (calibration and sample counts were performed at distances allowing consideration as point sources), and relative intensity (but not shielding) were reported for ^{224}Ra, ^{212}Pb, ^{212}Bi, and ^{208}Tl (radioactive progeny of ^{232}U that are assumed to be in secular equilibrium and have energetic gamma emissions with relatively high intensities). A standardized activity, A_S, for a particular spectral region of interest was determined from the equation

$$A_S = \frac{(A_M - B)}{R}\left(\frac{d_M}{d_S}\right)^2 , \qquad (1)$$

where A_M is the activity estimate, B is the background, R is the branching ratio for emissions associated with the nuclear transition, d_M is the sample (or unknown) source-to-detector distance at which the spectrum was recorded, and d_S is a standard source-to-detector distance.

^{232}U Decay Series

Nuclide	Half Life	Major Radiation Energies (MeV) and Intensities†		
		α	β (max)	γ
$^{232}_{92}$U	72 y	5.32 (68.6%) 5.27 (31.2%)	—	0.058 (0.2%)
↓				
$^{228}_{90}$Th	1.9 y	5.43 (72.7%) 5.34 (26.7%)	—	0.084 (1.2%)
↓				
$^{224}_{88}$Ra	3.6 d	5.68 (95.1%) 5.45 (4.9%)	—	0.241 (4.0%)
↓				
$^{220}_{86}$Rn	56 s	6.29 (100%)	—	—
↓				
$^{216}_{84}$Po	0.15 s	6.78 (100%)	—	—
↓				
$^{212}_{82}$Pb	10.6 h	—	0.16 (5.2%) 0.33 (85%) 0.57 (9.9%)	0.239 (45%) 0.300 (3.4%)
↓				
$^{212}_{83}$Bi	61 m	6.05 (25%) 6.09 (10%)	0.63 (3.4%) 0.73 (2.6%) 1.52 (8.0%) 2.25 (48.4%)	0.040 (2%) 0.727 (7%) 0.785 (1%) 0.893 (0.5%) 1.078 (0.8%) 1.620 (1.8%)
64% ↓				
$^{212}_{84}$Po	300 ns	8.78 (100%)	—	—
36% ↓				
$^{208}_{81}$Tl	3.1 m	—	1.28 (25%) 1.58 (21%) 1.80 (50%)	0.277 (6.4%) 0.763 (1.8%) 0.511 (23%) 0.583 (86%) 0.860 (12%) 2.614 (100%)
↓				
$^{208}_{82}$Pb	STABLE	—	—	—

† Intensities refer to percentage of decays of the nuclide itself.
Radiations with emission intensities less than 1% excluded.

R. L. Coleman | ORNL | 2002

Fig. 1. Radioactive decay series for ^{232}U.

The distance correction in Eq. (1) employs the Inverse Square Law in which emissions are presumed to reduce proportional to the square of the increase in distance from the source. The implications of this assumption will be addressed later in the Uncertainty discussion of Data Analysis.

The quantity A_M is determined in a given region of interest using the following relationships:

$$A_M = \frac{N}{\varepsilon\, t\, \gamma} = \frac{I_m}{\varepsilon\, \gamma} \quad , \tag{2}$$

where I_m is the measured photon intensity, N is the counts (net) observed in time t, ε is the detector efficiency in that energy region, and γ is the relative gamma-ray intensity (photons per disintegration) for the radionuclide at that energy.

2.3 Attenuation-Corrected Measurement Equation

Photon attenuation may be described (refs. 3, 4) by the expression

$$I = I_o e^{-\mu t} \quad , \tag{3}$$

where I is the photon intensity after transmission through an attenuating medium, I_o is the original unattenuated intensity, μ is the linear attenuation coefficient, and t is the thickness of the attenuating medium. This expression can be rearranged and restated as

$$\ln\left(\frac{I}{I_o}\right) = -\mu t \quad . \tag{4}$$

The attenuation coefficient represents the probability that a photon will interact with the attenuating medium. Interactions take place by three different processes in the energy range of interest here (from about 0.2 to 2.6 MeV). Low-energy photons (below about 0.25 MeV) interact predominantly by the photoelectric effect. Photons with energies above 0.25 MeV are attenuated primarily by Compton scattering until pair production becomes significant above about 3 MeV.

Each process is highly energy dependent, but μ can be shown to have an approximately linear relationship with $(1/E)^\alpha$ in this energy range.

$$\ln\left(\frac{I}{I_o}\right) = -\mu t \propto \left(\frac{1}{E}\right)^\alpha \quad . \tag{5}$$

Here, the exponent α empirically compensates for factors such as density and atomic number of the attenuating medium for many shielding materials. Table 1 gives values for the mass attenuation coefficient, μ/ρ , where ρ is the density (ref. 5) of common packaging materials (glass, aluminum, iron), germanium (from which the detectors used in this study are made), and uranium metal and uranium oxide (U_3O_8)—at theoretical densities. The regression of μ/ρ for iron against $1/E$ (where $\alpha = 1$) is shown in Fig. 2 and is approximately linear with a correlation coefficient of 0.989. Values for glass, aluminum, and germanium are very close to that for iron. The exponent α deviates from unity more significantly for high-atomic-number materials such as uranium and its oxides at their theoretical densities.

Table 1. Values of the mass attenuation coefficient for some common shielding materials*

	μ/ρ (cm^2/g)					
E (MeV)	Borosilicate glass ($Z_{eff} = 10.3$)	Aluminum ($Z = 13$)	Iron ($Z = 26$)	Germanium ($Z = 32$)	Uranium ($Z = 92$)	U_3O_8 ($Z_{eff} = 85.7$)
0.20	1.246E-01	1.22E-01	1.460E-01	1.661E-01	1.298E+00	1.116E+00
0.30	1.069E-01	1.04E-01	1.099E-01	1.131E-01	5.192E-01	4.554E-01
0.40	9.540E-02	9.28E-02	9.400E-02	9.327E-02	2.922E-01	2.618E-01
0.50	8.696E-02	8.45E-02	8.414E-02	8.212E-02	1.976E-01	1.805E-01
0.60	8.035E-02	7.80E-02	7.704E-02	7.452E-02	1.490E-01	1.384E-01
0.80	7.052E-02	6.84E-02	6.699E-02	6.426E-02	1.016E-01	9.684E-02
1.00	6.337E-02	6.15E-02	5.995E-02	5.727E-02	7.896E-02	7.660E-02
1.25	5.667E-02	5.50E-02	5.350E-02	5.101E-02	6.370E-02	6.266E-02
1.50	5.160E-02	5.01E-02	4.883E-02	4.657E-02	5.587E-02	5.525E-02
2.00	4.447E-02	4.32E-02	4.265E-02	4.086E-02	4.878E-02	4.813E-02
3.00	3.611E-02	3.54E-02	3.621E-02	3.524E-02	4.447E-02	4.315E-02

* Values of the atomic number Z for each element are provided for reference. The values of Z_{eff} for borosilicate glass and U_3O_8 are the effective atomic numbers, determined as described in ref. 3. Attenuation coefficients for U_3O_8 are a linear combination of coefficients for the constituent atoms, as prescribed by ref. 5.

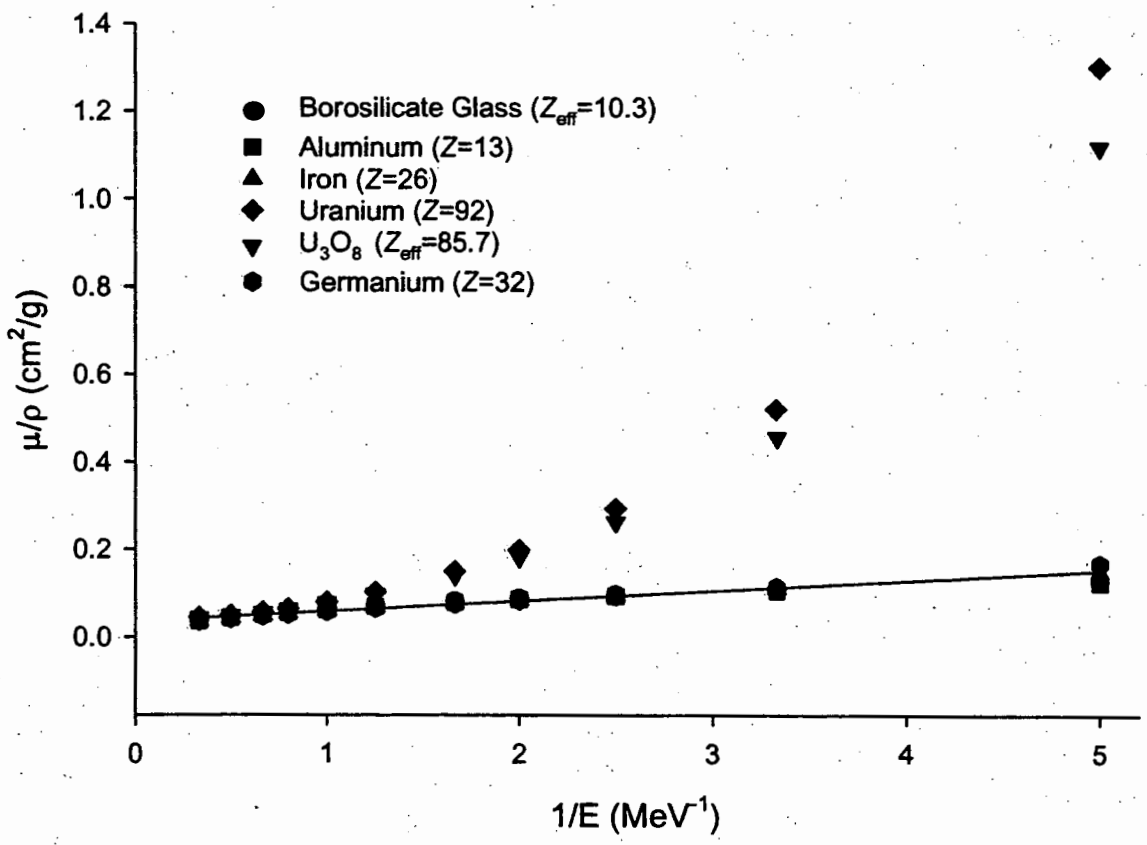

Fig. 2. Plot of the mass attenuation coefficient with 1/*E* for common packaging materials (glass, aluminum, iron), detector material (germanium) and uranium itself (U, U_3O_8). The regression line is for iron.

The linear attenuation coefficient μ has the same relationship with energy as the mass attenuation coefficient μ/ρ since density is constant for a given material. Similarly, the composite density for a given sample and its packaging is constant in a measurement. As will be shown later from the analysis of spectra, the μ/ρ for uranium compounds demonstrated a linear relationship with $1/E$ as opposed to the higher-order relationship typical of higher Z materials. This is believed to be a result of the lower bulk density typical of these materials (and typical of many process intermediates and products). However, it is expected that bulk uranium metals and high-density, pelletized oxides will behave in a non-linear manner, as indicated in Table 1 and Fig. 2.

For a given sample [with constant (but not necessarily homogeneous) absorber thickness and density], the regression of μ/ρ for iron (and other low-Z materials) against $1/E$ (described above) allows substitution for μ/ρ in Eq. (4) such that this equation becomes

$$\ln(I) \approx \ln(I_o) - c\left(\frac{1}{E}\right)^{\alpha} , \qquad (6)$$

where c is a constant of proportionality. Equation (6) can also be expressed as

$$\ln(A_S) \approx \ln(A_o) - c\left(\frac{1}{E}\right)^{\alpha} , \qquad (7)$$

where A_S [the standardized activity from Eq. (1)] is proportional to I (the photon intensity), and A_0 [the estimated (unattenuated) activity] is proportional to the original, unattenuated intensity. Equation (7) provides a useful expression in which spectrometry results are reported as radionuclide activity, rather than as photon intensities. A plot of the logarithm of activity estimated by Eq. (1) for a source radionuclide, based on the photon intensity at an energy E, against $(1/E)^{\alpha}$ would be approximately linear with slope c. For this linear function, the y-intercept equals $\ln(A_o)$, the logarithm of the source activity from the unattenuated photon intensity.

Figure 3 shows an example from a scan of high-quality (low-^{232}U-contamination) ^{233}U. For this material, three series of net-peak-area data could be obtained from the scan. The top line shows peaks associated with ^{233}U itself. The middle line shows ^{229}Th (the first decay product of ^{233}U) and its subsequent decay products (all of which are in equilibrium with ^{229}Th). The bottom line shows the decay products of ^{228}Th (the first decay product of the ^{232}U contaminant). The three lines are parallel within their statistical uncertainty (slope = -630±28 at 1σ), demonstrating a constant attenuation coefficient. The y-intercept for each line represents the log of activity for each of the three isotopes.

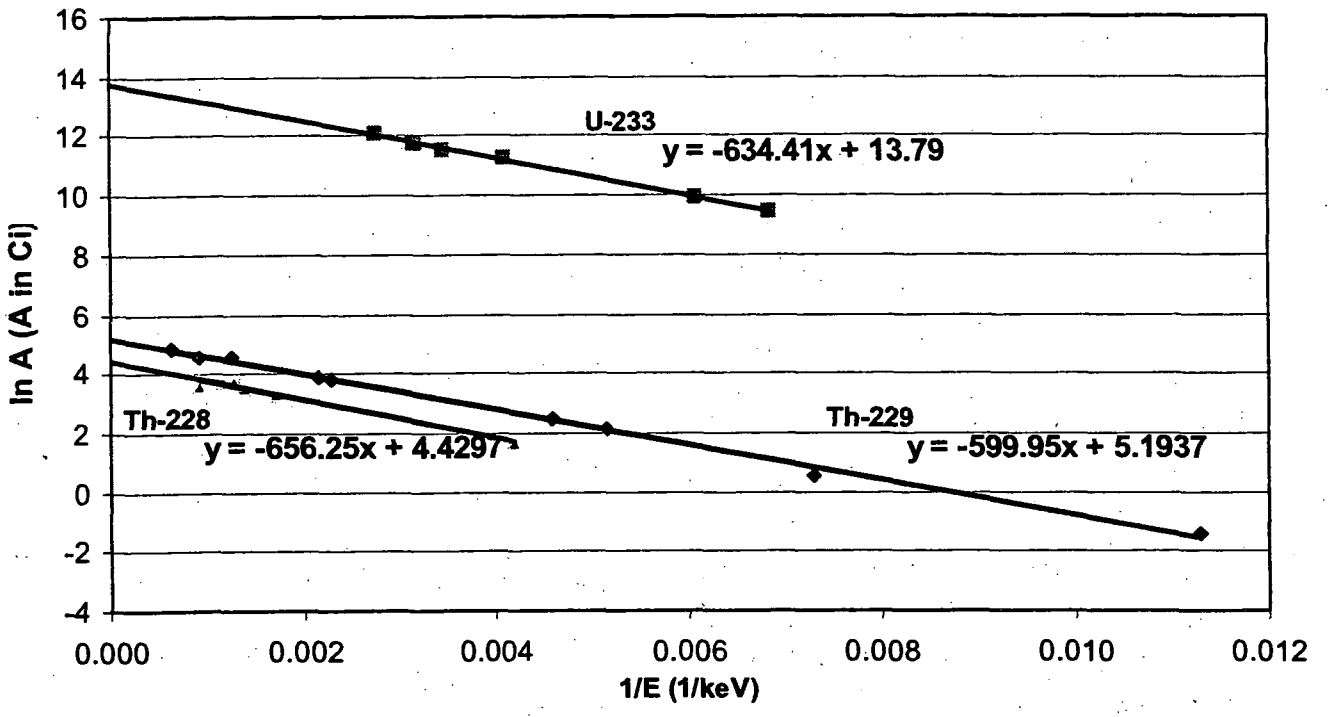

Fig. 3. Attenuation curves for high-purity ^{233}U.

2.4 Photon Peak Selections

Candidate peaks were identified conceptually using the on-line *Gamma-ray Spectrum Catalogue of Isotope Spectral Data*, maintained by the Idaho National Laboratory Gamma-Ray Spectrometry Center (INL; ref. 6; although several other sources may be used for this purpose). The usefulness of the candidate peaks depends on other nuclides present in the analyzed material and their impact on the spectral continuum in the energy region of interest. Potentially useful photons emitted directly from ^{233}U have energies less than 400 keV.

Studying the gamma spectra (ref. 6) for ^{232}U and ^{233}U reveals the difficulty of using photons emitted directly from ^{233}U. If isolated, these two nuclides emit photons at 487 discrete energies—three-fourths of which have energies less than 400 keV. If one includes additional radioactive impurities, the number

of discrete photons (and, thus the peak clutter) increases proportionally, thereby complicating peak deconvolutions.

Three ^{233}U photon peaks (e.g., at 291, 317, and 321 keV) show promise by having sufficient abundance to be well above the spectral continuum (for ^{232}U concentrations below ~20 ppm on a ^{233}U basis) and by appearing in a less cluttered region of the spectrum where *anticipated* source-related background will allow their resolution. Subsequent analysis of data has demonstrated that the 291-keV peak is more susceptible to source-related background than the other two ^{233}U peaks and was not identified reliably by the software analyzing the spectrum. This analysis also confirmed the advantage of using the higher-intensity 317-keV peak (over the 321-keV peak), allowing sufficient net peak areas to be accumulated in shorter periods (a useful goal for an operating process environment). If sufficient 321-keV net-peak-area data are accumulated, then its intensity can be compared to that for the 317-keV peak as a screen for the ^{233}U peak's validity.

Progeny in the ^{232}U decay chain have several intense gamma peaks that are easily resolved and quantified and that are in secular equilibrium with a long-lived precursor. These peaks range from 238 keV to 2,615 keV, thereby providing a broad energy range for modeling the attenuation of the matrix and packaging in which the material resides. Over a dozen distinct photopeaks from ^{232}U progeny, shown in Table 2, have been used (some more reliably than others) to help with this characterization.

Table 2. Gamma peaks from ^{232}U decay progeny

Energy (keV)	Nuclide
238.63	^{212}Pb
240.99	^{224}Ra
277.36	^{208}Tl
300.09	^{212}Pb
583.19	^{208}Tl
727.33	^{212}Bi
763.13	^{208}Tl
785.37	^{212}Bi
860.56	^{208}Tl
893.41	^{212}Bi
1093.90	^{208}Tl
1512.70	^{212}Bi
1620.50	^{212}Bi
2614.53	^{208}Tl

The longest-lived progeny of ^{232}U (half-life of 68 years) is ^{228}Th, its first decay product, with a 1.9-year half-life. A shorter-lived radioactive off-spring may be considered to be in secular equilibrium with its much longer-lived parent after about 5.5 (progeny) half-lives, or ~10.3 years in the case of ^{228}Th achieving equilibrium with ^{232}U. All succeeding progeny have half-lives of less than 4 days and are in secular equilibrium with ^{228}Th within a month. Since photopeaks from ^{228}Th itself are not used in characterizing attenuation, one needs only be certain that the material has aged at least 1 month since its last processing to ensure that the presumption of secular equilibrium is valid for modeling attenuation in this system of nuclides. In such case, ^{228}Th activity may be estimated directly. If aging also exceeds 10.3 years (as was the case for most items counted), then the activity of this decay chain's parent, ^{232}U, also may be estimated directly.

2.5 Estimating Activity

Since all items counted were aged well more than 10.3 years, secular equilibrium could be assumed between the ^{232}U parent and its progeny. Hence, the activity of ^{232}U in containers could be (and was) estimated directly by using the standardized activity, A_S of Eq. (1) determined from photon intensities at some or all of the photopeak energies in Table 2, as the dependent variable on the left-hand side of Eq. (7). Regression of $\ln(A_S)$ against $1/E$ (where $\alpha = 1$) by the method of least squares provided values for the slope, c, and y-intercept, $\ln(A_o)$.

With few exceptions, good functions were realized from linear regression based on the F-statistic and the Pearson product moment correlation coefficient, r. For counts yielding poorer correlations, the deviation appeared to be scattered and not conducive to a non-linear function as indicated in Fig. 2. The activity of ^{232}U could then be determined as the antilogarithm of the y-intercept.

Subsequently, the value of the slope was used in Eq. (7) with the standardized activity from analyzing the strongest photopeak of ^{233}U to determine its estimated activity at that line's y-intercept. [Had secular equilibrium between the parent (^{232}U) and its progeny *not* been ensured, then the ^{228}Th activity would have been represented by the y-intercept, $\ln(A_o)$, and its parent could have been estimated in a manner similar to that for ^{233}U (if there had been an available photopeak of ^{232}U) or by calculations considering in-growth and decay over the post-processing period.]

Five major steps were used to quantify ^{233}U in sample containers (primarily cans but also some drums):

1. Sample counting data were collected for containers of ^{233}U with up to 20 parts of ^{232}U contamination per million parts of ^{233}U (i.e., up to 20 ppm ^{232}U).

2. Counting data were analyzed to extract the net peak areas from background data and then were normalized for intensity using data libraries, yielding A_M.

3. Peak areas were corrected for branching using published values and were standardized to the distance at which the detectors were calibrated, yielding A_S.

4. The natural logarithm of A_S for ^{232}U, determined for each can from areas of selected photopeaks of ^{232}U progeny (see Table 2), was regressed against the inverse of the photon energies to arrive at the slope and intercept of Eq. (7). [A value of α different from unity may be selected when the linear regression of $\ln(A_S)$ against $1/E$ provides a poor fit (and indicates that a higher-order function will improve the fit. The best value of α may be found in such case by an iterative method that maximizes the F-statistic or correlation coefficient of the resulting regression of $\ln(A_S)$ against $(1/E)^{\alpha}$. This higher-order function was not warranted for any containers counted.]

5. Finally, the slope determined in Step 4 was used in Eq. (7) with the logarithm of ^{233}U activity determined at a discrete energy (and standardized as in Steps 2 and 3) to determine the intercept at $\ln(A_o)$ for which the antilogarithm is a direct indication of the ^{233}U quantity.

These steps were followed to evaluate each container of ^{233}U.

3. EQUIPMENT

The gamma spectroscopy system consists of three basic components: a detector unit and a portable spectroscopy system coupled to a windows-based computer for data analysis. The detector unit consists of an "n-type" high-purity germanium (HPGe) detector measuring 50 mm in diameter by 44 mm in length and integrated with a hybrid preamplifier and a high-voltage filter — all enclosed in a small cylinder about 3 in. in diameter by 9 in. in length. Integral to the detector unit is a compact cryostat, consisting of a liquid-nitrogen-filled Dewar which allows operation of the temperature-sensitive HPGe detector at any orientation.

The AMETEK® ORTEC® portable spectroscopy system uses the NOMAD™ Plus counting electronics coupled to a windows-based PC or laptop computer that share the functions of data acquisition, storage, display, and analysis. The NOMAD™ Plus hardware is a briefcase-sized unit that can operate by battery or line power. The computer uses ORTEC's GammaVision® software, version 5.3 (ref. 7) for interpretation, manipulation, and analysis of spectra.

4. DATA ANALYSIS

4.1 Results

Gamma spectra were collected from 35 experimental runs as a part of the ^{233}U Inspection and Repackaging Program at ORNL. Each of the 35 packages consisted of ^{233}U oxide or metal in a convenience can or jar, nested within one or two additional layers of metal packaging. (Each package of metals typically contained multiple small metal pieces as opposed to a single larger billet – effectively reducing its mass density.)

Because of operational constraints, spectra were collected as opportunities presented themselves for which, in most cases, the detector was several feet *above* the upright cylindrical canister — typically, a less-than-ideal counting configuration (especially for taller material loadings within a can). Other packages were counted from the side of the upright cylinder which, in some cases, were over packed in a DOT Type B shipping drum. Also due to operational considerations, spectra were collected for relatively short periods (typically less than 1 hour) which sometimes led to lower net peak areas than desired.

These materials had been in storage for over 15 years; hence, secular equilibrium between the ^{232}U contaminant and its progeny was assured. The ^{232}U concentration for the 35 counted packages ranged from 1 to 8 ppm ^{232}U on a ^{233}U basis. In material accounting, the ^{232}U content usually is considered in relative terms—as a quality factor for ^{233}U—using units of parts of ^{232}U per million parts of ^{233}U (expressed as ppm ^{232}U). Although these concentrations are considered low, they represent sufficient amounts (relative to the ^{233}U contents) to establish a pronounced Compton Continuum that reliably allowed resolution of only two photopeaks associated directly with ^{233}U progeny for which secular equilibrium among the nuclides could be assured. Therefore, the spectra for these packages were analyzed for the 14 peaks listed in Table 2 that are associated with ^{232}U.

Normalized activities were determined from net peak areas that were adjusted for distance (i.e., corrected to the detector calibration distance using the Inverse Square Law) and branching, and then plotted as a log function versus the inverse of energy. Linear regression determined [Eq. (7)] the slope and the y-intercept (which represented the log of the ^{232}U activity). A plot of this regression was shown previously (in Fig. 3) for three nuclides in one package.

Table 3 summarizes the results of ^{232}U activity determination for the 35 packages that were evaluated using the methodology. This set of results includes the counting configuration [i.e., the measurement distances (which factor into the adjustment for calibration distance) and the detector locations with respect to the upright cans: either above (top), to the side (side), or to the side of a can in a shipping drum (drum)]. Also provided are the trendline slopes, the spectra-estimated ^{232}U contents (in micrograms), the relative ^{232}U concentrations (in ppm ^{232}U relative to the spectra-estimated ^{233}U values), inventories of record, and the % errors.

Table 3. NDA results for ^{232}U
[sorted by % error (relative to record value)]

Can # *	Count configuration †	Measurement distance (in.)	Trendline slope	^{232}U content calculated from intercept (µg)	Relative ^{232}U concentration (ppm)	^{232}U from records (ppm)	% Error (relative to record value)
1048	Drum	90	-800.2	267	1.8	4.6	-61
1047	Drum	67	-800.0	109	1.9	4	-53
1045	Drum	78	-762.3	153	2.2	4.3	-49
1046	Drum	81	-829.5	182	2.2	4	-45
1105M	Side	44	-1727.0	230	4.6	8	-43
1099M	Side	60	-613.2	76	4.3	7	-39
1069	Side	76	-330.7	76	5.0	8	-38
1103M	Side	20	-332.3	13	5.3	8	-34
1064	Side	81	-299.4	88	2.9	4	-28
1044	?	78	-599.5	278	1.1	1.5	-27
1102M	Side	121	-523.7	363	5.9	8	-26
762	Top	178	-693.2	1953	5.5	7	-21
765	Top	178	-388.5	1432	5.5	7	-21
766	Top	178	-734.3	1326	5.5	7	-21
768	Top	178	-791.4	1601	5.5	7	-21
764	Top	207	-538.3	3071	5.7	7	-19
1067	Side	70	-355.1	25	4.1	5	-18
763	Top	207	-718.3	2166	5.8	7	-17
1070	Side	20	-296.7	10	5.8	7	-17
1068	Side	70	-393.2	327	6.7	8	-16
771	Drum	206	-936.2	749	5.9	7	-16
773	Top	207	-1326.1	830	6.0	7	-14
767	Drum	195	-878.6	980	6.1	7	-13
770	Top	167	-780.0	1201	6.1	7	-13
772	Top	178	-906.7	1514	6.3	7	-10
1063	Side	20	-206.5	7	6.3	7	-10
1065	Side	81	-371.4	57	3.6	4	-10
1073	Top	70	-339.1	85	3.6	4	-10
769	Drum	186	-730.5	1823	6.6	7	-6
1080	Side	119	-532.2	316	4.3	4.5	-4
1072	Top	178	-452.7	259	6.7	7	-4
1066	Side	20	-357.4	4	4.6	4	15
1071	Top	207	-474.4	1487	9.5	7	36
1079	Side	119	-527.7	171	3.3	2.4	38
1098	Top	207	-544.9	2903	22.6	8	183

* Suffix: M = Contents are metal form (all other contents are oxides).

† Count Configurations: "?" = undocumented configuration; Top = a count of an upright can from above; Side = a count of an upright can from the side; and Drum = a side count through the side of a drum.

A quick review of the data shows rough general agreement (with one exception) between ^{232}U concentration calculated from the spectra and those in the record. The exception is Can 1098, for which the spectrum indicated almost three times the record value for ^{232}U. It should be noted that the inspection of this package indicated probe radiation readings consistent with the spectrum-estimated ^{232}U content (casting doubt on the record value).

Although some agreement is noted above, further review of the data shows relatively significant errors between ^{232}U concentration calculated from the spectra and those in the record. Ignoring the single outlier noted above, these errors range from -61% to +38% with an apparent bias in those errors representing an underestimation of relative ^{232}U concentration calculated from the spectra by somewhere between -13% (mean value) to -18% (median value). Two major factors not related directly to the spectrometry results are *known* to contribute to these errors:

- The record values were not adjusted for decay (at the 69-year half-life) of ^{232}U. This adjustment alone would reduce these errors by decreasing record values at least 15% for >15-year-old material and even in excess of 30% for the oldest items. This single adjustment could essentially eliminate the apparent bias. Since precise decay times were not available for all items, the original record values were retained.

- The record values were determined in an analytical laboratory by relative alpha activities (between ^{232}U and ^{233}U) and typically were reported to only one significant digit. Single-digit ppm levels inherently introduce between 5% and 50% uncertainty in the reported value. That is, a 9 ppm record value actually could be any value between 8.5 and 9.5 ppm – introducing up to a 6% error – while a 1 ppm record value actually could be any value between 0.5 and 1.5 ppm – introducing up to a 50% error from the record value. Again, this uncertainty by itself could explain much of the errors noted above.

It should be noted that an alternative method of estimating relative ^{232}U concentrations (i.e., in ppm ^{232}U units) substantiated the calculated results (i.e., estimated from the spectra) in Table 3. This alternative method uses a ratio of the 300.09-keV peak for ^{212}Pb to the 317.16-keV peak for ^{233}U. These two peaks are sufficiently close in energy to allow direct comparison of their activities with minimal concern for differences in attenuation.

Quantities of ^{233}U then were estimated using Eq. (7) along with the slopes from the linear regressions for ^{232}U and values for A_S determined from data collected at the most prominent ^{233}U photopeak (317.16 keV). The quality of this peak in a given spectrum may be validated by comparing the area of this peak with those of two other ^{233}U peaks (at 291.35 and 320.54 keV) for expected peak ratios determined from their relative intensities. These peak ratios and the "goodness-of-fit" parameters (r^2) were used as initial screens to confirm the validity of the spectra as they were applied to Eq. (7). It should be noted that, with very few exceptions (due to the prevalent Compton Continuum and the aforementioned operational constraints), only a few peaks (usually only two peaks) emanating directly

from ^{233}U were available consistently (i.e., with sufficient net peak areas) for use in directly generating a regression equation. Therefore, using the slope from the ^{232}U regression was required.

Spectra from several packages were rejected early in the evaluation process for a variety of reasons that were quickly evident from an initial review of data. Typically, spectra were rejected due to insufficient 317-keV net peak areas (operations for some packages required only ^{233}U peak identification, not statistical evaluation) or poor 317-keV peak shape (typically indicating electronic gain shift during the count). These early rejections are not included in the following discussion or tabulations.

Table 4 summarizes the results of ^{233}U quantity determinations for the 35 packages that were evaluated using the methodology. This set of results indicates the count configuration [i.e., the measurement distance (factoring into the adjustment for calibration distance) and the detector location with respect to the upright can: either above (Top), to the side (Side), or to the side of a can in an upright shipping drum (Drum)]. Also provided is the trendline slope, the estimated ^{233}U content calculated from each can's gamma spectrum, inventory of record for each can, and the error (both relative and absolute) of the estimated content related to the record value.

It is important to note that the data collected for the runs in Tables 3 and 4 were adjusted in a consistent manner, as described above. No manual adjustments were made for special cases; this restriction was imposed in support of the minor objective to use readily available output of existing spectral analysis software as direct input to this methodology. [Some adjustments were attempted in parameters used by the automatic data processing features (e.g., library peak match width which is used in identifying peaks compared with library entries) to determine if a change would improve the results for *all* data sets. However, no consistent benefit resulted in quantity estimates for any attempted adjustments.]

4.2 Uncertainty

Uncertainty in the estimate of activity depends on uncertainties in the standardized activities (A_S) of Eq. (1). Total uncertainty in A_S consists of combined uncertainties from random and systematic contributions. The random components of uncertainty in Eq. (1) are in the activity, A_M, and in the background, B, as provided by the software.

The reported activity also includes a systematic component of uncertainty in the choice of gamma-ray photon intensities, γ, used to normalize the results. Reported values of γ for photon emissions used in this report are provided in Table 5. These are taken from three commonly used references of photon energies and intensities: the *Nuclear Data Sheets* (ref. 8), *Evaluated Nuclear Structure Data File* (ref. 9), and "The Gamma Rays of the Radionuclides: Tables for Applied Gamma Ray Spectrometry" (ref. 10). The software version used for evaluating gamma-ray spectra in this report uses data from ENSDF. Significant discrepancies in reported values of γ are not uncommon, especially for low-intensity photons.

Table 4. NDA results for ^{233}U
[sorted by % error (relative to record value)]

Can # *	Count config-uration†	Measurement distance (inches)	Trendline slope	^{233}U Calc'd from slope & 317-KeV peak (g)	^{233}U from records (g)	% Error (relative to record value)	Absolute error (g)
773	Top	207	-1326.1	139.3	607	-77.1	-467.7
1046	Drum	81	-829.5	83.5	185.9	-55.1	-102.4
1047	Drum	67	-800	56.2	122.5	-54.1	-66.3
771	Drum	206	-936.2	127.3	272	-53.2	-144.7
770	Top	167	-780	197.9	404	-51.0	-206.1
767	Drum	195	-878.6	160.2	323.1	-50.4	-162.9
1045	Drum	78	-762.3	70.4	132.7	-47.0	-62.3
1048	Drum	90	-800.2	146.2	266.9	-45.2	-120.7
1102M	Side	121	-523.7	61.3	99	-38.1	-37.7
1105M	Side	44	-1727	50.3	80	-37.1	-29.7
1098	Top	207	-544.9	128.3	198	-35.2	-69.7
769	Drum	186	-730.5	275.9	415	-33.5	-139.1
772	Top	178	-906.7	238.7	342	-30.2	-103.3
768	Top	178	-791.4	289.6	391.8	-26.1	-102.2
766	Top	178	-734.3	240.9	324.1	-25.7	-83.2
1099M	Side	60	-613.2	17.9	24	-25.4	-6.1
763	Top	207	-718.3	374.3	487.2	-23.2	-112.9
762	Top	178	-693.2	355	461.6	-23.1	-106.6
1044	?	78	-599.5	262.6	269.3	-2.5	-6.7
1071	Top	207	-474.4	157	160	-1.9	-3
1079	Side	119	-527.7	51.3	49	4.7	2.3
1072	Top	178	-452.7	38.4	36	6.8	2.4
1063	Side	20	-206.5	1.1	1	10.3	0.1
764	Top	207	-538.3	541.9	479	13.1	62.9
1080	Side	119	-532.2	74.2	61.5	20.7	12.7
765	Top	178	-388.5	262	216	21.3	46
1068	Side	70	-393.2	48.5	40	21.3	8.5
1103M	Side	20	-332.3	2.5	2	27.0	0.5
1069	Side	76	-330.7	15.3	11	39.3	4.3
1065	Side	81	-371.4	16	10.8	48.4	5.2
1070	Side	20	-296.7	1.6	1.1	48.5	0.5
1066	Side	20	-357.4	0.8	0.5	55.7	0.3
1073	Top	70	-339.1	23.4	15	56.0	8.4
1067	Side	70	-355.1	6.2	3.8	63.7	2.4
1064	Side	81	-299.4	30.1	18	67.5	12.1

* Suffix: M = Contents are metal form (all other contents are oxides).

† Count Configurations were: "?" = undocumented configuration; Top = a count of an upright can from above; Side = a count of an upright can from the side; and Drum = a side count through the side of a drum.

Table 5. Reported gamma-ray intensities*

Energy (keV)	Nuclide	Literature Source		
		ENSDF	NDS	Erdtmann and Soyka (ref. 10)
238.63	^{212}Pb	0.433 (3)	0.433 (3)	0.431
240.99	^{224}Ra	0.0410 (5)	0.0397 (4)	0.039
277.36	^{208}Tl	0.0631 (9)	0.0636 (9)	0.0650
300.09	^{212}Pb	0.0328 (3)	0.0757 (7)	0.0327
583.19	^{208}Tl	0.845 (7)	0.852 (7)	0.860
727.33	^{212}Bi	0.0658 (5)	0.1027 (8)	0.118
763.13	^{208}Tl	0.0181 (5)	0.0183 (5)	0.017
785.37	^{212}Bi	0.0110 (1)	0.0172 (2)	0.020
860.56	^{208}Tl	0.1242 (10)	0.1253 (10)	0.120
893.41	^{212}Bi	0.0038 (2)	0.0059 (3)	0.0066
1093.90	^{208}Tl	0.0040 (3)	0.004	0.0038
1512.70	^{212}Bi	0.0029 (4)	0.0029	0.0057
1620.50	^{212}Bi	0.0149 (3)	0.0232 (5)	0.0275
2614.53	^{208}Tl	0.9916	1.000	1.00
291.35	^{233}U	0.0000537 (5)	0.0000537 (5) †	0.000160
317.16	^{233}U	0.0000776 (7)	0.0000776 (7) †	0.000231
320.54	^{233}U	0.0000290 (3)	0.0000290 (3) †	0.000087

*Values are the number of γ photons per decay. Uncertainty (1 standard deviation) in the last digit, where reported, is given in parentheses.

†These values, which are reported incorrectly in *Nuclear Data Sheets*, Vol. 59, No. 1 (1990), are taken from the original reference cited by NDS.

Examination of Table 5 reveals notable differences in some values in even the more recent references (refs. 8, 9). The uncertainty introduced through values of γ is systematic and difficult to estimate, since differences are between results from different laboratories using equipment, isotopic sources, and procedures peculiar to each. Uncertainties provided by the spectral analysis software are considered applicable to values of A_M.

Non-random components of uncertainty in Eq. (1) are in the branching ratio and source-to-detector distances. The branching ratio, R (for which only the ^{208}Tl photon peaks from the α decay of ^{212}Bi are

assigned a value different from unity), is a value taken from the literature and does not vary in these measurements. As a result, its uncertainty component is constant (systematic). The calibration standard's source-to-detector distance, d_S, is determined at the time of calibration and also does not vary within or between measurements. Together, these systematic components appear to contribute to a bias reflected in the results. The measurement source-to-detector distance (d_M; at which a spectrum is recorded for the sample to be estimated) is the same for all photon peaks within a spectrum. Therefore, uncertainties in source-to-detector distances also are constant (systematic) for each analysis; however, since it is determined individually for each analysis, it is considered random among the collection of analyses.

It is noted that the component of error for measurement source-to-detector distance (d_M) can be a dominant error for volume-distributed sources, which is the case for containers studied in this report. As noted earlier, net peak areas used in each count were adjusted using the Inverse Square Law to correct the measurement distance to the calibration distance. The Inverse Square Law assumes a point source for the emissions. While the source used for calibration realistically *was* a point source (an invisible speck sandwiched between two thin layers of plastic), the material counted as samples had measurable bulk (typically up to 3½ inches in diameter by up to 1 foot in length). This bulk distributes the source inconsistently within the container (e.g., sometimes involving multiple pieces or multiple inner cans). Source distribution can be a dominant source of uncertainty for improperly described sources due to its impact on the source-to-detector distance. This impact may be discussed in terms of source depth and source offset from the surface normal to the detector.

For the counts used in this study, source depth provided the larger component of uncertainty. Source-to-detector distance corrections were made using measured container-to-detector distances and radiographic images to visually approximate the center of source bulk within the container. Since the bulk approximation was not performed rigorously, an uncertainty of up ½ inch is considered a reasonable for the side counts and up to 1 inch for top counts. For side counts of maximum 3½-inch-diameter cans, the ±½-inch uncertainty could introduce up to a 6% error for a count taken at a minimum 44-inch distance. For top counts of up to 1-foot source depth, the ±1-inch uncertainty could introduce up to a 3% error for a count taken at a minimum 70-inch distance. (See Table 4 for counting distances and configurations.)

Uncertainty introduced by not correcting source offset from the surface normal to the detector is related to the cosine of the angle formed at the detector by the photon path from offset and the assumed path length normal to the source surface. This error will be significant if the spectra are acquired with the detector positioned at distances from the source that are on the order of the longest dimension of the source. Except for four cans containing only a few grams (thereby requiring shorter detector-to-sample distances to achieve higher count rates and reasonable count times for the operating environment), the minimum counting distance was 44 inches. Side counts involved cans only up to 8 inches tall (all 1-foot-tall sources were counted from a top orientation) having material that could occupy up to 7 inches of that external height. If one uses the worst case in which the entire source is located at the furthest point from the surface normal (but still along the can centerline), then the photon flight path to the

detector would be 44.1 inches [or $(3.5^2 + 44^2)^{1/2}$] which could only introduce errors that are less than 1%. Top counts introduced even smaller uncertainties since the counting distances were larger and the maximum offset distances were smaller.

Therefore, the overall impact of treating samples with volume-distributed sources as if they were point sources potentially introduced ~6% total uncertainty into quantity estimates.

Operational constraints prevented running a series of controlled experiments to determine individual components of uncertainty not provided automatically by the software or discussed in a bounding context above. However, some statistical indicators are provided in Table 6. A crude, partial indication of uncertainty was estimated using the standard uncertainty of two key components: the slope [c in Eq. (7)] generated for each count and the standardized activity for the ^{233}U peak [representing the uncertainty of $\ln(A_S)$ for ^{233}U]. The variances of these two components were combined in Table 6 (column 4) to indicate the variance of the intercept after the curve was translated to intersect with the ^{233}U standardized measurement at $\ln(A_S)$. At the intercept, the uncertainty is considered merely a crude partial estimate of the uncertainty for ^{233}U as $\ln(A_o)$.

4.3 Discussion of Results

Some general observations can be made about these results:

1. Larger quantities of similar materials (e.g., metals, oxides) yielded larger negative slopes.

2. Larger quantities yielded higher F-statistics and r^2 values (i.e., had better linear fits for the data).

3. Items counted through a shipping drum tended to show larger underestimations of content.

4. Items containing larger quantities of material that were counted from the top tended to show underestimation more often than items containing smaller quantities and items counted from the side.

The first two observations tend to validate a major premise of the methodology that was demonstrated by essentially parallel curves in Fig. 3: Energy-dependent photon attenuation can be modeled directly and empirically from typical gamma spectra. The second observation also reflects better statistics that become available with relatively short counts of larger quantities of radionuclides.

The third and fourth observations point toward additional studies that are needed, and may infer some limitations for using the energy-dependent photon attenuation for quantitative determination. Both of these observations relate to some attenuation characteristic either imposing a correlation that is not recognized, or having an effect on the methodology that is not understood fully.

Additional studies are warranted to determine if a material thickness is being exceeded above which ***no*** photons (or a statistically insignificant number of photons) in the regions of interest are reaching the

detector. Portions of material from which no photons reach the detector would underestimate the quantity being measured (which may underlie the fourth observation above).

Table 6. Some uncertainties related to estimated ^{233}U quantities

[sorted by % error (relative to record value)]

Can # *	Std. distr. of the intercept (%)	Std. distr. of the 317-keV peak (%)	A Partial estimate of uncertainty (%) †	^{233}U Calc'd from slope & 317 key peak (g)	% error (relative to record value)	F-statistic	r-squared goodness of fit (from 0 to 1)
773	0.0121	0.3326	33.3%	139.3	-77.1	681	0.984
1046	0.0089	0.0454	4.6%	83.5	-55.1	688	0.984
1047	0.0139	0.0628	6.4%	56.2	-54.1	300	0.965
771	0.0053	0.0692	7.0%	127.3	-53.2	1820	0.994
770	0.0076	0.1442	14.4%	197.9	-51.0	559	0.981
767	0.0062	0.1515	15.2%	160.2	-50.4	1090	0.990
1045	0.0074	0.0387	3.9%	70.4	-47.0	871	0.988
1048	0.0073	0.0298	3.1%	146.2	-45.2	881	0.988
1102M	0.0274	0.0804	8.5%	61.3	-38.1	25	0.692
1105M	0.0135	0.5010	50.1%	50.3	-37.1	1229	0.991
1098	0.0037	0.0800	8.0%	128.3	-35.2	972	0.989
769	0.0034	0.0546	5.5%	275.9	-33.5	2292	0.995
772	0.0056	0.0692	7.0%	238.7	-30.2	1313	0.992
768	0.0059	0.0663	6.7%	289.6	-26.1	907	0.988
766	0.0063	0.0411	4.2%	240.9	-25.7	705	0.985
1099M	0.0038	0.0771	7.7%	17.9	-25.4	2578	0.996
763	0.0052	0.0472	4.8%	374.3	-23.2	891	0.988
762	0.0051	0.0568	5.7%	355	-23.1	887	0.988
1044	0.0118	0.0290	3.1%	262.6	-2.5	184	0.944
1071	0.0046	0.0811	8.1%	157	-1.9	541	0.980
1079	0.0092	0.0776	7.8%	51.3	4.7	264	0.960
1072	0.0608	0.0752	9.7%	38.4	6.8	4	0.269
1063	0.0152	0.0515	5.4%	1.1	10.3	40	0.785
764	0.0064	0.0213	2.2%	541.9	13.1	308	0.966
1080	0.0092	0.0523	5.3%	74.2	20.7	232	0.955
765	0.0048	0.0296	3.0%	262	21.3	337	0.968
1068	0.0161	0.0846	8.6%	48.5	21.3	41	0.789
1103M	0.0181	0.0386	4.3%	2.5	27.0	57	0.838
1069	0.0099	0.0645	6.5%	15.3	39.3	111	0.910
1065	0.0211	0.0766	8.0%	16	48.4	33	0.752
1070	0.0194	0.0628	6.6%	1.6	48.5	45	0.803
1066	0.0748	0.1392	15.8%	0.8	55.7	7	0.375
1073	0.0140	0.0870	8.8%	23.4	56.0	57	0.837
1067	0.0299	0.0890	9.4%	6.2	63.7	19	0.638
1064	0.0122	0.0531	5.5%	30.1	67.5	57	0.839

*Suffix: M = Contents are metal form (all other contents are oxides).

†Uncertainty estimates contain contributions only from the intercepts and the 317-keV peaks.

5. CONCLUSIONS

A promising technique for nuclear material quantity determination is presented that allows gamma emissions to be used directly to model attenuation in matrices of radioactive materials. The model then may be used directly to indicate the quantity of radioactive material and/or may be applied to quantify other commingled radioactive materials in the matrices.

The quantitative determination is the result of a simple, straightforward method that uses energy-dependent photon attenuation to model empirically (and to correct for) the package attenuation from typical gamma spectra emitted from within. This correction is made possible by analyzing emissions from one or more nuclides, in this case progeny of ^{232}U, and then applying that correction to commingled materials, such as ^{233}U (which always coexist with ^{232}U in varying relative concentrations). This technique is applicable for materials in which a nuclide (and/or its progeny) provide a broad spectrum of gamma photopeaks. If these photopeaks represent nuclides that are in secular equilibrium with a longer-lived nuclide in the decay chain, then a predictable relationship emerges between the measured activity from a particular emission and the energy of that emission. This relationship has the form

$$\ln(A) = \ln(A_o) - c(1/E)^{\alpha} \quad . \tag{8}$$

The slope, c, and exponent, α, of this relationship model a composite of the attenuating nature of the material's matrix and packaging. The intercept at $\ln(A_o)$ represents the logarithm of activity (as if unattenuated) for the nuclide in secular equilibrium with its progeny. The slope and exponent of this function allow the subsequent estimation of activity (as if unattenuated) of other radionuclides in the mixture from indicated activity of their associated photopeak(s) (e.g., 317.16 for ^{233}U). The content of other nuclides in the container may, therefore, be determined directly using this method.

Although the goal of this work is to provide a technique for determining or *verifying* inventory values, its development thus far has provided estimation of contents that can be used for *confirming* inventory values (a less precise measure than verification) or that can be used in quantifying wastes (rather than inventoried material). However, this technique is not yet mature for inventory quantity determination or verification. Future studies will implement sample rotation to minimize many geometric effects, and may incorporate photon flux-leakage modeling to compensate for volume-distributed sources, as warranted. Parametric studies are warranted to determine the effects of counting configuration on mass estimates and to determine material thicknesses (including both media and packaging) which, if exceeded, would allow essentially *no* photons (or a statistically insignificant number of photons) in the regions of interest (emanating from beyond that thickness) to reach the detector, thereby underestimating quantities. Controlled experiments also are needed to determine all components of error so that their effect may be incorporated into a rigorous uncertainty statement for a given estimate.

The existence of high-energy (>1 MeV) photons (in the ^{232}U decay chain) represents a two-edged sword in this methodology. On one hand, it is beneficial in that is provides photons which (to some extent) should penetrate the full length of the matrix and packaging material. That is, for the package configurations tested, one may reasonably expect to detect a high-energy (MeV-level) photopeak with a net area that is proportional to the amount of contained material. On the other hand, the high-energy photons impose a pronounced Compton Continuum (or background) that inhibits accumulating meaningful net areas of photopeaks in the sub-MeV range for counts of relatively short duration. The use of newer detectors and/or software employing Compton suppression techniques should substantially reduce this component of background and improve the quality of data collected for short-duration counts (always a goal of operating organizations).

This technique may be applied generically to radioactive materials for which there is an associated set of photons providing a similarly useful (i.e., broad-energy-range) spectrum with known relative photon intensities for characterizing attenuation presented by the material's matrix and packaging. Known relative intensities may be anticipated, for example, where members in a decay chain are in secular equilibrium or where known ratios of gamma-emitting materials are present as a result of past processing.

6. REFERENCES

1. Hagenauer, R. C., and R. L. Mayer II, *Nondestructive-Assay Quantification of Poorly Characterized Radioactive Isotopes* (copy available on-line from AMETEK® ORTEC® directly or at their World Wide Web site at http://www.ortec-online.com/).

2. *In Situ Gamma Spectroscopy with ISOCS, an In Situ Object Counting System*, an Application Note from Canberra® Industries (available from Canberra® directly or from their World Wide Web site at http://www.canberra.com/).

3. Gollnick, D. A., *Basic Radiation Protection Technology,* 4th Ed., Pacific Radiation Corporation, Altadena, Calif., October 2000.

4. Knoll, G. F., *Radiation Detection and Measurement,* 2nd Ed., John Wiley & Sons, New York, 1979.

5. Hubbell, J. H., and S. M. Seltzer, "Tables of X-Ray Mass Attenuation Coefficients and Mass Energy-Absorption Coefficients," NISTIR 5632, available on the World Wide Web at http://physics.nist.gov/PhysRefData/XrayMassCoef/cover.html.

6. Idaho National Engineering and Environmental Laboratory Gamma-ray Spectrometry Center, On-Line Catalogues, *Ge(Li)-Si(Li) Gamma Spectrum Catalogue*, updated by J. R. Davidson, published March 29, 1999. Current edition available on the World Wide Web at http://www.radiochemistry.org/periodictable/gamma_spectra/.

7. *Gamma-Ray Spectrum Analysis and MCA Emulator for Microsoft® Windows® 95, 98, and NT® Software User's Manual*, Software Version 5.2 (A66-B32), PerkinElmer™ Instruments, ORTEC® Products, Oak Ridge, Tenn.

8. Nuclear Data Sheets **47**(4), 800 (April 1986).

9. *Evaluated Nuclear Structure Data File*, maintained at the National Nuclear Data Center of Brookhaven National Laboratory and accessible on the World Wide Web at <http://www.nndc.bnl.gov/nndc/ensdf/>. Spectral information from ENSDF is also available in ref. 8.

10. Erdtmann, G., and W. Soyka, "The Gamma Rays of the Radionuclides: Tables for Applied Gamma Ray Spectrometry," in *Topical Presentations in Nuclear Chemistry*, Vol. 7, Verlag Chemie, New York, 1979.

INTERNAL DISTRIBUTION

1. C. W. Alexander
2. S. T. Baker
3-7. J. S. Bogard
8. J. M. Begovich
9. M. E. Borum
10. M. W. Burgess
11. K. A. Carney
12. C. W. Coates
13. R. L. Coleman
14. T. B. Conley
15. S. E. Fisher
16. T. W. Forrester
17. I. G. Gross
18. P. F. Gubanc
19. R. T. Jubin
20. D. N. Kovacic
21-25. A. M. Krichinsky
26. G. R. Larson
27. S. C. Marschman
28. E. S. Meyers
29. M. E. Murray
30. C. V. Parks
31. B. D. Patton
32. J. E. Powell
33. B. A. Powers
34. A. W. Riedy
35. H. Y. Rollen, Jr.
36. J. E. Rushton
37. S. E. Smith
38. W. J. Toth
39. R. M. Wham
40. J. M. Whitaker
41. M. C. Wright
42. Laboratory Records — RC

EXTERNAL DISTRIBUTION

43-47. P. J. Bereolos, Select Engineering and Contracting, Inc., 11825 Yarnell Road, Knoxville, TN 37932
48. L. D. Boggs, US Department of Energy, P.O.Box 2001, MS-EM-90, Oak Ridge, TN 37831
49. N. E. Brandon, Isotek Systems, LLC, 700 South Illinois Ave, SuiteA102, Oak Ridge, TN 37830
50. B. C. DeMonia, US Department of Energy, P.O.Box 2001, MS-EM-921, Oak Ridge, TN 37831
51. J. K. Gilpin, Bechtel Jacobs Company LLC, 1 Bethel Valley Road, Bldg CT6-7500, MS-6400, Oak Ridge, TN 37830
52. L. L. Gilpin, Isotek Systems, LLC, P.O.Box 2008, MS-6046, Oak Ridge, TN 37831
53-57. A. J. Lucero, Western Research Institute, 365 N. 9th Street, Laramie, WY
58. S. H. McCracken, US Department of Energy, P.O.Box 2001, MS-EM-90, Oak Ridge, TN 37831
59-63. C. S. Scheffing, 1208 Lincoln Park Blvd., Kettering, OH 45429
64. F. Schultz, Northwest Nuclear LLC, 212 N. Watt Road, Knoxville, TN 37922